Ann. Geophysicae 13, 583–594 (1995) © EGS – Springer-Verlag 1995

Annales Geophysicae

The use of a model current wedge in the determination of the position of substorm current systems

M. Cramoysan, R. Bunting, D. Orr

Department of Physics, University of York, Heslington, York Y01 5DD, UK

Received: 1 September 1993/Revised: 3 November 1994/Accepted: 29 November 1994

Abstract. We present a technique for determination of the position and extent of the current systems present during substorm breakup. The parameters of a three-dimensional model of the currents are determined by fitting the model to data from the SAMNET magnetometer array, a midlatitude array of seven stations. The model used is a fully 3D current wedge aligned along dipolar field lines, the parameters being the meridians of upward and downward field-aligned currents (FACs), the latitude of the auroral electrojet and the magnitude of current growth over the observation interval. The method is novel in that the three geometrical parameters are first determined with the fourth arrived at via a secondary process. It has been applied to a number of events and appears to make estimates of the longitudes of the FACs consistent with the predictions of previous methods. Since the method employs a fully 3D model of the substorm current wedge as opposed to an idealised 2D model, it is reasonable to place more reliance on the results so obtained. Moreover, the method also has the additional benefit of a prediction of the latitude of the substorm electrojet and the nature of the current growth through the wedge at substorm onset.

1 Introduction

The substorm current wedge (McPherron *et al.*, 1973) has been widely used to model the gross magnetic observations made on the Earth's surface during the breakup phase of the magnetospheric substorm. This model current system consists of field-aligned currents (FACs) linking the auroral ionosphere with the equatorial tail of the magnetosphere, joined by a westward-directed auroral electrojet, and closed by an eastward directed tail current. This closed system, when added to the prior westward tail current amounts to a diversion of this current through the ionosphere (Fig. 1). Simplified versions of this current system have been successfully used by Lester *et al.* (1983, 1984, 1989) to put some order into substorm-associated pulsation characteristics. These models associate certain features of the ground magnetic signature with the meridians of the FACs and the central meridian of the wedge itself.

The actual wedge could best be characterised by specifying the geometry of the FACs and the spatial variation of the currents flowing. This would involve a large number of parameters. The middle ground between such a complete specification and the simple models used by Lester *et al* (1983, 1984, 1989) is to consider a wedge in a strictly dipolar field which is fully characterised by four parameters. Apart from the meridians of the FACs, these are the latitude of the ionospheric portion of the current circuit, and the actual current flowing. Attempts have been made to determine these parameters directly from the observed data using mathematical techniques, with some degree of success (Horning *et al.*, 1974; Richmond and Kamide, 1988; Richmond *et al.*, 1988). It is the purpose of this paper to detail a variation on this approach whereby the three geometrical parameters are first computed independently from a secondary process which yields the current parameter. The technique has been applied to data from the SAMNET array of magnetometers, and verified against data from the EISCAT Magnetometer Cross. The method produces estimates of the longitudes of the FACs consistent with results obtained by previous methods. Considering that a fully 3D model is employed as opposed to a simplified 2D model it is concluded that the results should be more reliable. Moreover, estimates are also given of both the current flowing in the wedge and the latitude of the electrojet.

2 The method

The first stage in the development of the method is to explore the correlations between pairs of time series of magnetic components at different pairs of stations.

Correspondence to: D. Orr

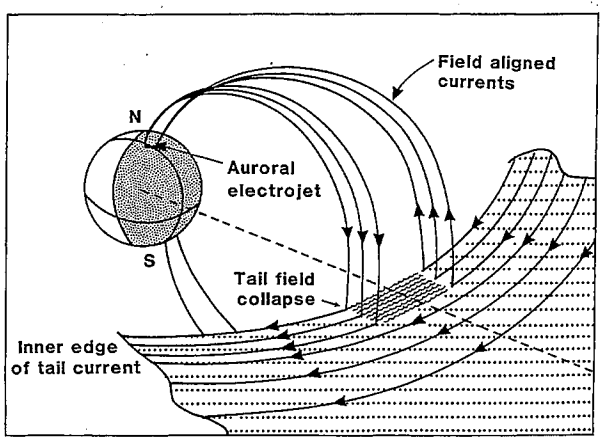

Fig. 1. The geometry of the 3D current wedge system (McPherron *et al.*, 1973)

The field observed on the ground due to an arbitrary 3D current system may be represented by

$$F(t) = F_0 + i(t) f(\theta, \phi, t) + e(t), \tag{1}$$

where F_0 represents an unknown DC offset, $i(t)$ is the time variation of the total current flowing through the system, $f(\theta, \phi, t)$ is the unknown geometrical function relating unit total current to ground position, and $e(t)$ is a noise function. Within the context of this paper, the term 'noise' refers to a combination of strictly local effects from each station and other sources, such as the field due to other current systems, not associated with the substorm current wedge. An approximation may be applied whereby the geometrical function relating the position of the current system to the observational station is assumed to be constant in time. The only variation is due to the variation of the currents flowing in the system. This has been dubbed the corotating approximation since it is equivalent to assuming that the wedge is rotating with the Earth. Two datasets, $F_A(t)$ and $F_B(t)$, each having the form of Eq. 1, may be plotted against each other, and under the corotating approximation the best fit straight line through the data may be shown to give a least squares gradient (m) given by

$$2m = -\frac{f_A}{f_B}(1-z) + \frac{f_B}{f_A}(1+z) + \frac{\overline{e_A^2} - \overline{e_B^2}}{f_A f_B}, \tag{2}$$

where

$$z = \sqrt{1 + \frac{(\overline{e_A^2} - \overline{e_B^2})((\overline{e_A^2} - \overline{e_B^2}) + 2(f_A^2 - f_B^2(\overline{i^2} - \overline{i}^2))}{((f_A^2 + f_B^2(\overline{i^2} - \overline{i}^2))^2}}, \tag{3}$$

and the correlation coefficient is

$$r = \frac{1}{\sqrt{1 + \dfrac{\overline{e_A^2}}{f_A^2(\overline{i^2} - \overline{i}^2)}}} \cdot \frac{1}{\sqrt{1 + \dfrac{\overline{e_B^2}}{f_B^2(\overline{i^2} - \overline{i}^2)}}} \leq 1. \tag{4}$$

Assuming that the difference of the magnitudes of the two noise terms is small in relation to the signal from the current system, the gradient simplifies to

$$m = \frac{f_B}{f_A}. \tag{5}$$

Regarding the nature of the current variation, the only assumption is that the current does actually vary in time. Any significant noise components cause a departure of the correlation coefficient from unity.

The next stage is to find the set of geometrical parameters which minimises the differences between a series of experimental and modelled gradients. Since the two data sets of the form of Eq. (1) can just as well be different components at the same station as either like or unlike components at different stations, across even a limited array of magnetometers there can be a substantial number of observations. For example, in the case of seven observatories there are 91 pairs of horizontal magnetic field components to correlate. Model field deviations were computed by integrating the effects of unit current elements spaced along the wedge following the method of Kisabeth and Rostoker (1977) using a Romberg method. The parameter fit was performed by minimising the squared differences between the experimental and modelled data ratios, normalised to the magnitude of the experimental ratio, that is, a deviation function (D)

$$D = \sum \left(1 - \frac{R_m}{R_d}\right)^2, \tag{6}$$

where R_m and R_d are the modelled and experimental ratios respectively, and the summation was over all station/component pairs. The differences were also weighted in two ways. The first weight compensated for the calculable effect of either or both stations rotating underneath the model field, that is, it biased against parameter sets where the corotating approximation was a poor one. The change in the ratio over the course of the measurement (r) was calculated and used to weight the differences according to the function

$$W_s = e^{-(\mathrm{mod}(\delta r/r))}. \tag{7}$$

Furthermore, noise on either of the datasets would affect the reliability of the gradient. As demonstrated by Eq. (4), the correlation coefficient gives a convenient indication of the presence of noise. This was also used to weight the differences. The results of the optimisation process are best demonstrated using a variety of case studies.

3 Case studies

3.1 Day 237, 1990

In this case study we start by following the method through to give the desired parameters. After that we provide independent evidence which supports the results obtained. SAMNET (Yeoman *et al.*, 1990) comprises a 2D array of seven fluxgate magnetometers in northern Europe (Fig. 2). These operate with a resolution of 0.25 nT and a sampling rate of 5 s, more than adequate for the study of

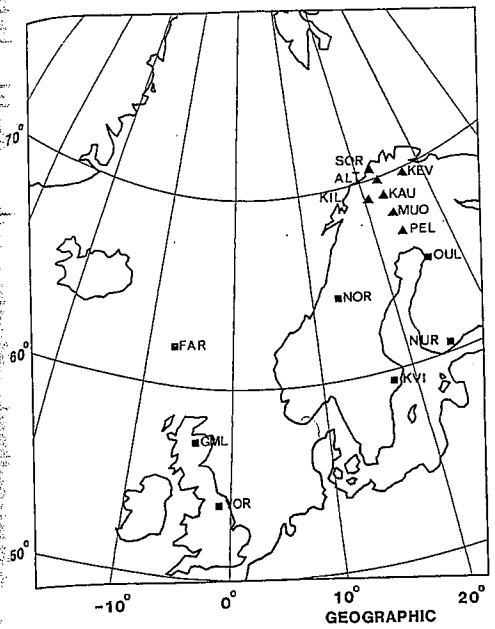

Fig. 2. Map showing the locations of the SAMNET stations and the EISCAT Magnetometer Cross sites

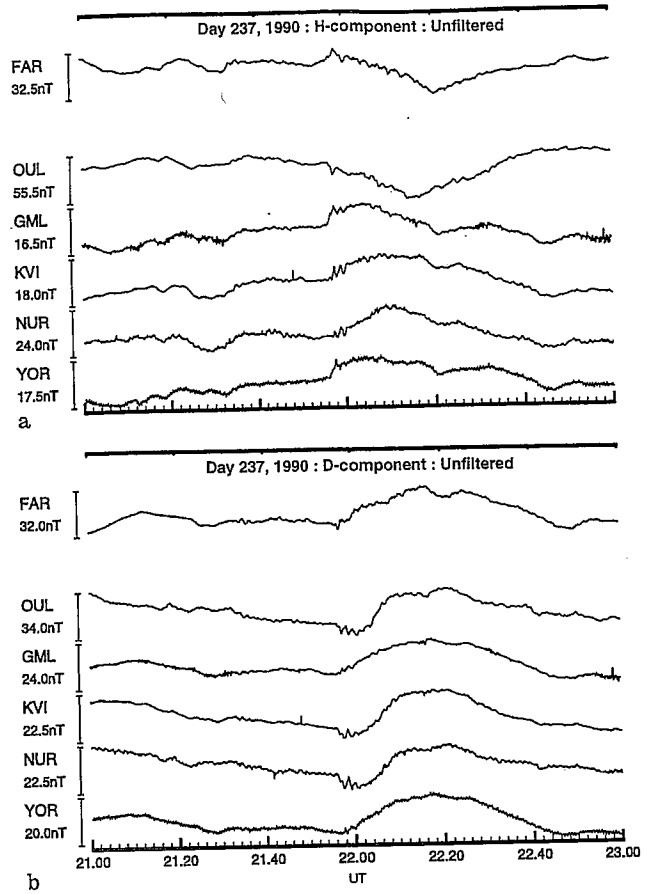

Fig. 3a, b. Unfiltered magnetograms for the Day 237, 1990 event as observed on the SAMNET array. Nordli was not available during this event. The analysis interval was from 21:56 to 22:01 UT

substorm disturbances. Figure 3 shows unfiltered magnetograms from the SAMNET magnetometer array for a substorm that occurred on Day 237, 1990. NOR was not available during this event. There is pronounced pulsation activity superimposed on longer duration variations. The analysis was performed over the interval 21:56 to 22:01 UT after application of a 200-s low-pass filter, this filter preventing any signals in the Pi1 or Pi2 frequency bands from influencing the result. Throughout this study a visual inspection suggested that the Z-component was strongly affected by local induction effects which did not seem to manifest themselves in the horizontal components. As such in all cases to date the analysis was made on the basis of just the H-and D-component data.

The best-fitting model parameter set was that which gave the minimum weighted mean squared deviation (MWMSD) between model and data. FACs were considered at a spacing of 0.25 h (3.75°) across 12-h (180°) range spanning SAMNET, and L-shells with an interval of 0.25 between $L = 5$ and $L = 10$. The FAC meridians were referenced to a fixed longitude of 90°E geomagnetic, approximately central with the array. For this event the MWMSD was 0.22, that is the mean squared difference between data and model taken across all available station/component pairs was 0.47. In general it was found that a MWMSD below 1 indicated a reasonable fit, and a figure below 0.25 corresponded to an excellent fit. The optimum parameters were L-shell of 5.75 with FAC meridians of -1.75 and $+2.00$ h of local time. For this event these equate to a downward FAC at 64° and an upward FAC at 120°. Figure 4 gives a qualitative impression of the degree of reliability of these estimates. In each case, for a range of possible values of the parameter, the MWMSD is calculated subject to the restriction of this one parameter. The optimum set should be characterised by

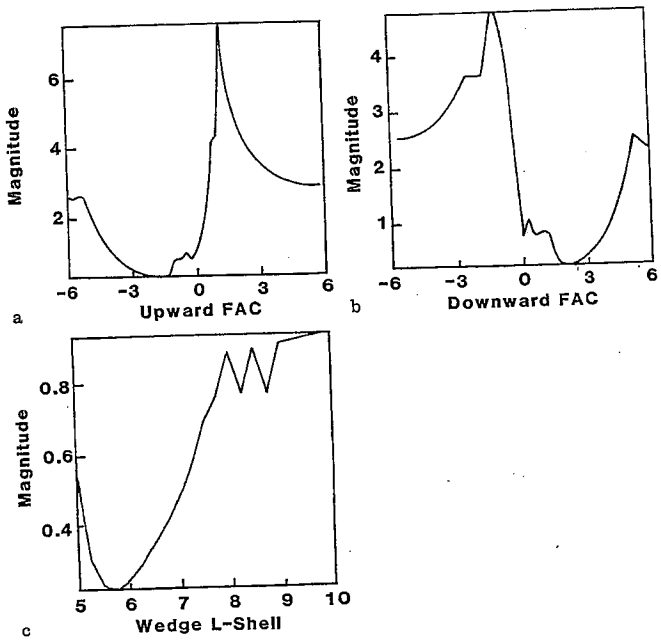

Fig. 4a–c. Model deviations projected onto each parameter axis for the Day 237, 1990 event. For values along the x-axis of each graph the minimum deviation between model and data was evaluated through optimisation of the other two parameters alone

a well-defined minimum with a gradual increase on either side, the sharper the rate of increase on either side, the more reliable the estimate. The results for both FACs show very clear minima, the MWMSDs rising rapidly for parameter sets away from this optimum. The L-shell, however, is less well defined. For any L-shell between $L = 5$ and $L = 10$ it is possible to find a pair of FACs yielding a MWMSD below 1. Thus, although the optimum value of $L = 5.75$ is well defined, the uncertainty is greater than with the other two parameters.

The next stage is to determine the fourth parameter, the current variation over the observation interval, the first element of which is to obtain separate estimates based on each component at each station. A straight line was fitted to each component using a least squares approach, the gradient of such a line multiplied by the observation period giving a measure of the deviation at each station. Dividing this deviation by that due to a unit current flowing through the wedge located above gives an estimate of the current change. An independent estimate was produced for each component at each station, giving 12 estimates in this case, one from each of two components at six stations. Table 1 summarises the results and serves to show how these must be interpreted. The first pair of columns details the total field variation across the event determined as above. The second pair gives the results of dividing this into the modelled value of each component at each station, that is, the current change across the event based on each component in turn. Ideally all 12 estimates would be identical. However, that based on the FAR H-component gives a much lower figure (actually 0.004 MA). This is because over the analysis interval FAR happened to be in an area where the H-component due to the wedge happened to be very small. Thus the small signal from the wedge was easily swamped by geomagnetic noise or other non-substorm related variations. Indeed, the average variation of -0.3 nT is comparable with the ± 0.25 nT resolution of the magnetometers employed in SAMNET. A single estimate of the rate of current change was obtained simply by averaging the individual component or station values, with appropriate weighting to offset results obtained from unreliable data. The best fit current was a variation of 0.072 MA across the event, corresponding to a rate of change of 0.014 MA min^{-1}.

Table 1. Average field deviations for each components at each station for the Day 237, 1990 event. Individual wedge current estimates from each component based on the best fitting wedge. Data from NOR was not available for this event

Station	Modelled field per MA current (nT)		Experimental field deviation (nT)		Current change (MA)	
	H	*D*	*H*	*D*	*H*	*D*
FAR	−76.1	83.8	−0.3	8.6	0.00	0.10
OUL	−125.0	−78.8	−10.4	−6.1	0.08	0.08
GML	63.7	80.6	4.3	5.5	0.07	0.07
KVI	61.5	−22.6	5.3	−1.6	0.09	0.07
NUR	54.2	−61.3	4.4	−4.3	0.08	0.07
YOR	68.3	61.0	4.9	4.4	0.07	0.07

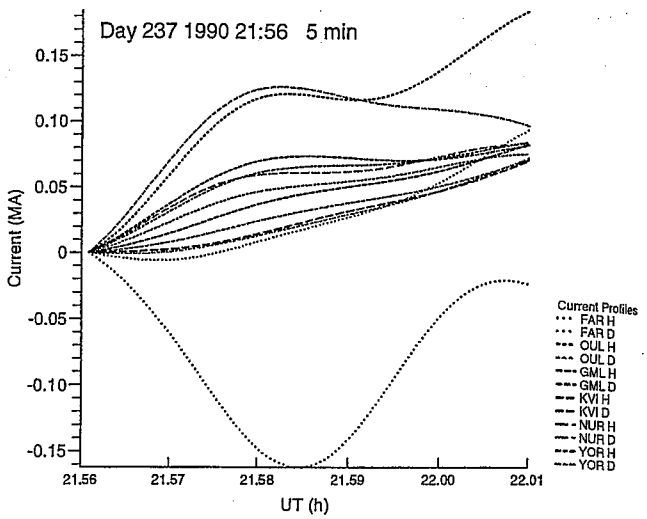

Fig. 5. Superimposed current development profiles from all available stations for the Day 237, 1990 event. Each individual profile corresponds to one component from one station. The lowest profile corresponds to the data from FAR H-component which only varied by about 0.3 nT throughout the event, and the highest profile corresponds to the KVI D-component which only varied by 1.6 nT

An alternative way of examining the current flow at onset was to plot a profile showing the time variation. A very similar process to that detailed above was used except that rather than using a single average figure for the variation of each component, the raw time series was used giving a profile from each component at each station. The 12 such profiles are shown in Fig. 5. Ideally all the profiles should be identical but 2 of the profiles appear to be significantly different from the rest. These apparent anomalies have the same cause as those explained above. The apparently anomalous lowest profile was due to the FAR H-component which as shown above only varied by 0.3 nT across the course of the event. The upper profile, also apparently anomalous, corresponds to the KVI D-component, which had an associated variation of -1.6 nT. In fact, the best current wedge model for this event has a zero in the H ground field close to FAR, and a zero in D close to KVI. These stations which have only a low magnitude magnetic variation due to the substorm wedge can be strongly influenced by other current systems. Thus both of these profiles are easily reconciled. All the other stations and components had variations of 4.5 nT or greater, giving much greater reliability.

Once all four of the wedge parameters had been determined, the next task was to decide on their validity. Using the method employed it was not possible to assign limits of accuracy to each parameter but it was possible to obtain an overall figure of merit for the set as a whole. This was accomplished by substitution of the optimum parameter set back into the model to directly compare it with the data. Using the average current determined above, the expected ground field is directly compared with the observational data in Fig. 6. In each case the discrete points represent the experimental data from Table 1, whilst the continuous and broken lines detail the variation

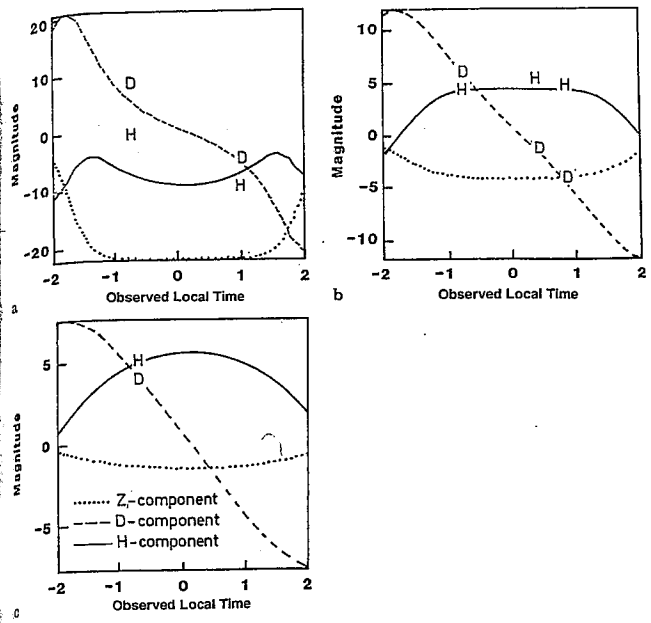

Fig. 6a–c. Comparison between experimental and modelled data for the Day 237, 1990 event. In each case a pair of symbols *H* and *D* represent the field deviations measured at a station, while the *solid* and *dashed lines* represent the modelled fields derived from the optimum parameter set (21:56–22:01 UT). The experimental data are from **a** FAR (left) and OUL (right); **b** GML (left), KVI (centre) and NUR (right); **c** YOR

of the field based on the parameters determined above. The plots are separated into three groups each of approximately constant geomagnetic latitude, in each case the model profile corresponds to the geomagnetic latitude averaged across the appropriate stations. The RMS difference between model and experimental data was 1.7 nT. A measure of the quality of fit may be obtained by normalising this according to the mean field magnitude seen across the array. In this case this quality factor was 0.35.

The main source of inaccuracy between the modelled and experimental data was probably what can best be termed noise. By this we refer to a combination of strictly local effects such as interference or hardware noise and other effects such as the influence of non-substorm associated geomagnetic variations. There may also be components due to the enhancement of the driven current system, and to the dynamics of the onset, which will not be well modelled if the current injection positions vary by significantly more than our resolution of 2° in longitude. The solution of this problem requires a time-varying version of the model, which is the subject of further work. It is in the nature of the method employed that the noise component will manifest itself most significantly in the final stage of the process during determination of the current change. From Eq. (2) and (3) there will be either partial or total cancellation of noise signals between station pairs. As such the first stage of the method produces an estimate of the wedge location largely independent of these noise factors. The current estimate, however, is arrived at directly from the source data at each station and is thus affected by such noise factors. Thus a poor agreement at this stage is more likely due to uncertainties in the current parameter rather than the geometrical ones.

The last stage was to obtain some independent corroboration of some of the parameters determined above. The *Z*-component changes sign very close to the electrojet, being positive to the north and negative to the south. By comparing the predictions of the optimum parameter set with *Z*-component data from a chain straddling the electrojet, the reliability of the model may be checked. For this event, data was also available from the EISCAT Magnetometer Cross (Lühr *et al.* (1984), Figs. 2 and 7). Experimental deviations for these stations were derived by straight-line fitting in the same manner as before and using the best-fit current derived from the SAMNET stations; the data is compared with the model in Fig. 8. It is evident that there is only fair agreement in the field magnitudes. However, the model used consists of an electrojet of infinitesimal latitudinal extent. The actual electrojet would extend over at least a few degrees of latitude

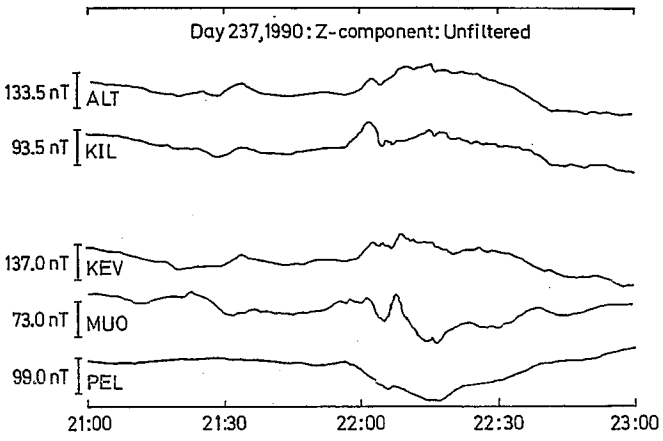

Fig. 7. Unfiltered *Z*-component magnetograms for the Day 237, 1990 event as observed by the EISCAT Magnetometer Cross

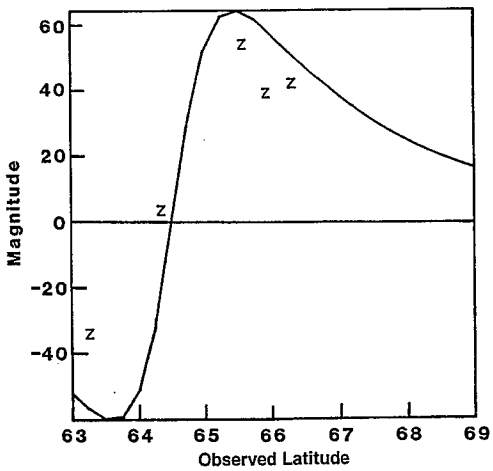

Fig. 8. Comparison between EISCAT Magnetometer Cross and data derived from the optimum parameter set. The solid line gives the modelled data as determined solely by consideration of the SAMNET stations. The *Z* symbols represent field deviations for the stations PEL, MUO, KEV, KIL, and ALT, respectively (from left to right)

which would have the effect of decreasing the rate of change from positive to negative Z-values. It may be shown that the sharpness of the switch from regimes of positive to negative Z is strongly dependent on the latitudinal extent of the current system, but that the latitude of zero field strength is little affected, as in Fig. 8. Both modelled and experimental Z-components agree well on a latitude near 64.5 N.

3.2 Day 100, 1988

Unfiltered magnetograms for an event on Day 100, 1988 are given in Fig. 9. Again there is clear pulsation activity superimposed on bay-like disturbances. An analysis was performed over the interval 0:26 to 0:39 UT with a 200-s low-pass filter. The MWMSD for this event was 0.07 indicating an excellent fit.

The analysis results of Fig. 10 indicate a well-defined L-shell of $L = 5.25$, an extremely well-defined downward FAC west of the reference point by 0.25 h of relative local time, and a poorly-defined upward FAC well to the west of the array at or beyond 6 h. The corresponding meridians are 86° and 0° geomagnetic. Wedge current estimates (Table 2) for the event are very consistent right across the array and for all components at all stations the field

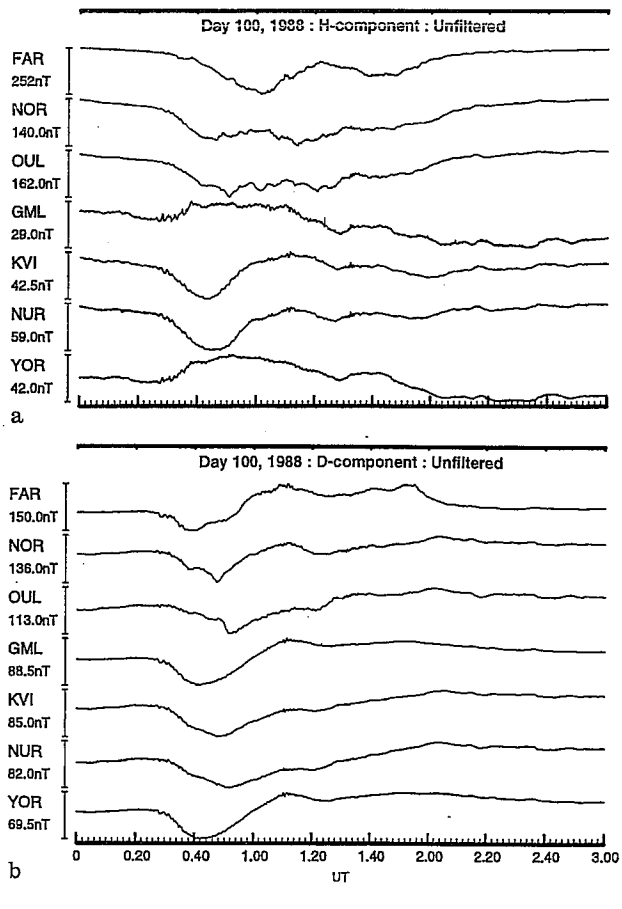

Fig. 9a, b. Unfiltered magnetograms for Day 100, 1988 as observed on the SAMNET array. The observation interval was from 0:26 to 0:39 UT

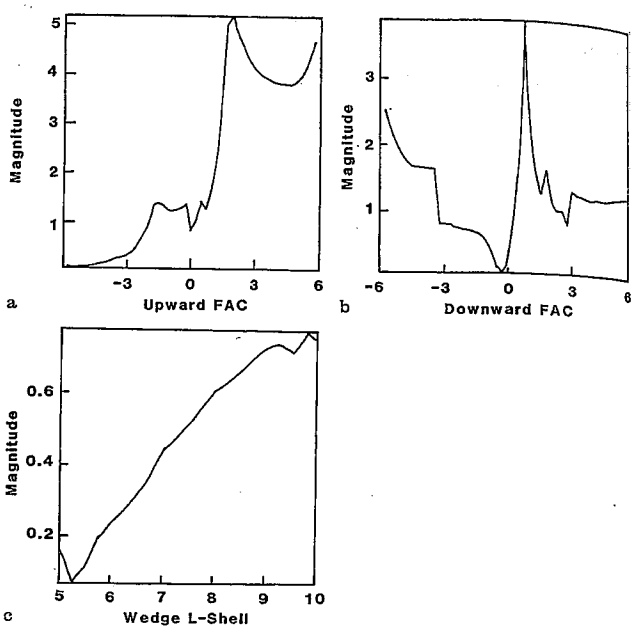

Fig. 10a–c. Model deviations projected onto each parameter axis for the Day 100, 1988 event

changes seen are large enough for these current estimates to be reliable. A best-fit current growth of 0.36 MA through the event corresponds to a growth rate of 0.028 MA min^{-1}. The experimental and modelled data are compared in Fig. 11a–c. The RMS deviation between the two is 7.3 nT with a corresponding quality factor of 0.18; in other words, a very good fit. The current profiles for this event (Fig. 12) again show a steady increase after a more gradual onset. All the profiles are fairly consistent as would be expected considering that the experimental fields are all of a reasonable magnitude (Table 2).

3.3 Day 258, 1988

Magnetometer data for this event are shown in Fig. 13. The Pi2 pulsations (Fig. 14) show an initial onset at 01:44 UT, followed by a second onset at ~01:51. The unfiltered data show a comparatively weak deviation in the easterly stations of the array, while the western meridian chain (FAR, GML, YOR) shows stronger effects, particularly in the H-component. This initially suggests a distant current growth to the west of the array. In contrast, the much stronger bays associated with the second onset indicate a closer current system.

Analysis of the first onset was carried out using the model over the interval 01:44 to 01:49 UT, and showed a moderate level of model fitting, with a MWMSD of 0.86. The analysis results (Fig. 15) give a well-defined downward field aligned current position at 1.75 h west in local time, while the more distant upward field aligned current is less well defined at 2.25 h west. The wedge L-shell value is poorly defined at $L > 8.5$. This parameter set corresponds to a narrow wedge between ~56°E and ~64°E geomagnetic, and at a high latitude, which is in agreement with the initial prediction.

Table 2. Field deviations and wedge current estimates for the Day 100, 1988 event

Station	Modelled field per MA current (nT)		Experimental field deviation (nT)		Current change (MA)	
	H	*D*	*H*	*D*	*H*	*D*
FAR	120.0	−168.0	−43.5	−63.7	0.36	0.38
OUL	−202.0	−145.0	−76.4	−55.9	0.38	0.39
NOR	−115.0	−54.6	−63.4	−19.1	0.55	0.35
GML	31.9	−139.0	10.1	−49.0	0.32	0.35
KVI	−66.4	−138.0	−25.8	−39.6	0.39	0.29
NUR	−76.8	−97.7	−37.7	−27.5	0.49	0.28
YOR	40.4	−110.0	18.5	−41.9	0.46	0.38

Table 3a. Field deviations and wedge current estimates for the Day 258, 1988 event, 01:44–01:49 UT

Station	Modelled field per MA current (nT)		Experimental field deviation (nT)		Current change (MA)	
	H	*D*	*H*	*D*	*H*	*D*
FAR	1.47	−27.9	−0.1	−7.1	−0.09	0.25
OUL	−7.47	−14.7	−0.6	−2.5	0.08	0.17
NOR	−6.61	−9.09	0.6	−3.8	−0.08	0.42
GML	6.18	−14.2	2.6	−3.5	0.42	0.25
KVI	−1.91	−11.2	0.4	−2.9	−0.22	0.26
NUR	−3.12	−9.37	−0.4	−2.4	0.12	0.26
YOR	5.89	−9.72	3.4	−2.9	0.58	0.30

Table 3b. Field deviations and wedge current estimates for the Day 258, 1988 event, 01:51–01:57 UT

Station	Modelled field per MA current (nT)		Experimental field deviation (nT)		Current change (MA)	
	H	*D*	*H*	*D*	*H*	*D*
FAR	23.7	−177.0	5.0	−35.0	0.21	0.20
OUL	−90.3	−113.0	−22.7	−22.2	0.25	0.20
NOR	−63.1	−53.5	−21.9	−16.2	0.35	0.30
GML	51.1	−89.9	12.4	−20.3	0.24	0.23
KVI	−23.1	−88.4	−5.4	−18.6	0.23	0.21
NUR	−33.3	−68.4	−12.1	−15.8	0.36	0.23
YOR	46.0	−61.9	14.9	−17.3	0.32	0.28

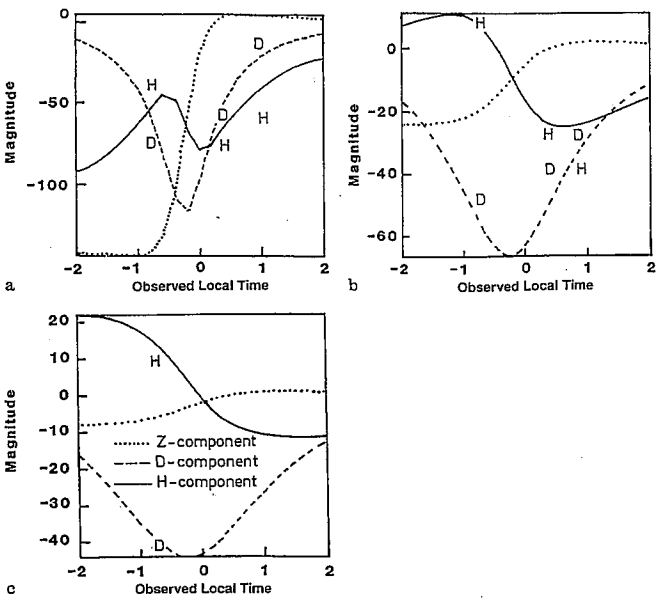

Fig. 11a–c. Comparison between experimental and modelled data for the Day 100, 1988 event. The experimental data are from **a** FAR, NOR, OUL; **b** GML, KVI and NUR; **c** YOR

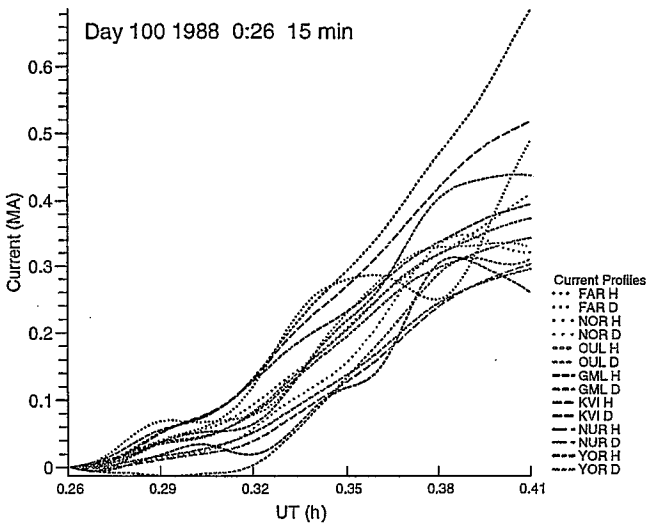

Fig. 12. Superimposed current profiles for the Day 100, 1988 event

Since the effects of the first onset on our array are small, a separate analysis can be carried out on the second onset, from 01:51 to 01:57 UT. This gives a much better MWMSD of 0.12, as would be expected given the larger signal present. The resulting best fitting parameters are at 3.0 h west MLT for the upward FAC, 0.5 h west for the downward FAC and an *L*-shell value of 6.25 (Fig. 16). In this case, the wedge is wider, from 45°E geomagnetic for the upward FAC to 82.5°E for the downward, and also closer to the array in its latitude, corresponding to ~66.5°N geomagnetic.

The equivalent current curves are given in Fig. 17. The results are generally consistent with current growth, but show inconsistent growth rates for those stations where the magnetometer deviation is small, due either to the distance of the current wedge, or to their being close to a minimum position in the ground magnetic field due to that wedge. The data from these stations would be expected to receive more interference from non-substorm related geomagenetic signals and thus will have received low weighting within the analysis, relative to data from other stations (Sect. 2).

In Fig. 17a, for the first onset, with small signals, the agreement between stations is less good than in Fig. 17b, where all but one of the current curves are consistent with a steadily increasing wedge current rate averaging 0.038 MA min^{-1} over the 5-min analysis interval.

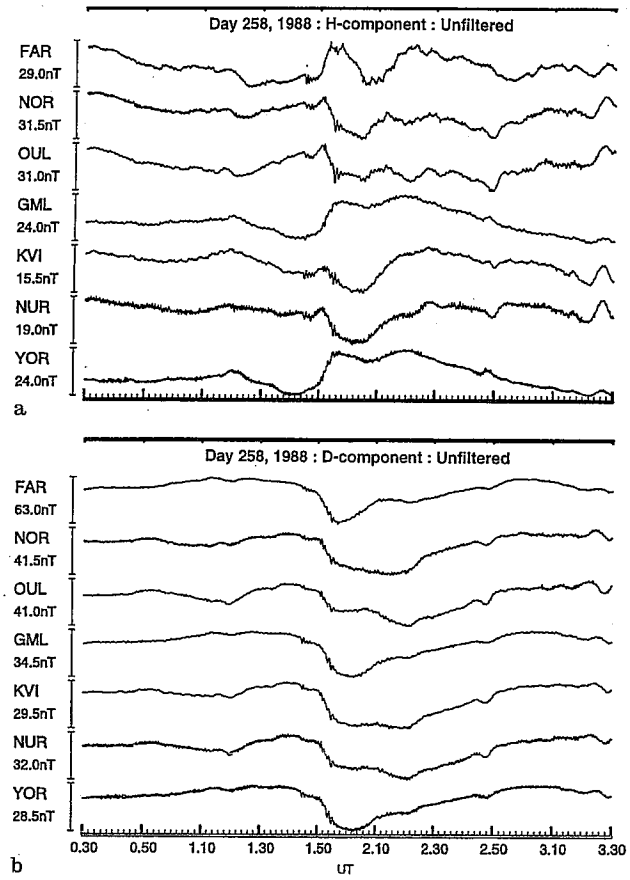

Fig. 13a, b. Unfiltered magnetograms for the Day 258, 1988 event as observed by SAMNET, **a** for the *H*-component, and **b** the *D*-component. Two onsets have been analysed, the first beginning at 01:41, the second at 01:57 UT

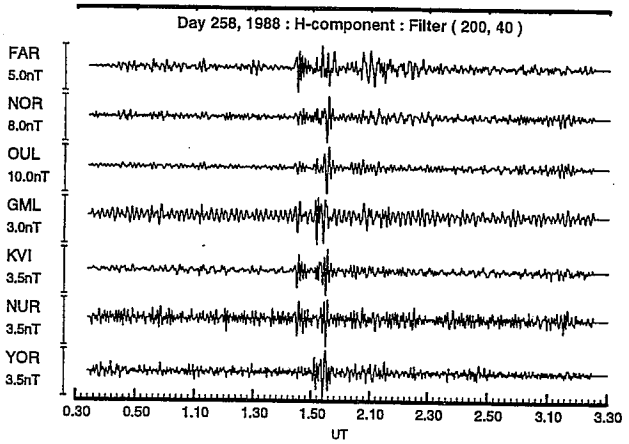

Fig. 14. High-pass filtered SAMNET *H*-component magnetogram showing Pi2 pulsations during the Day 258, 1988 event

4 Comparisons with previous wedge location methods

Fifty-one events were analysed from the SAMNET magnetometer array. These consisted of 11 events examined in a previous study by Yeoman (1988) and a further 41 events distributed through 1988, 1989 and 1990. Of these, 38

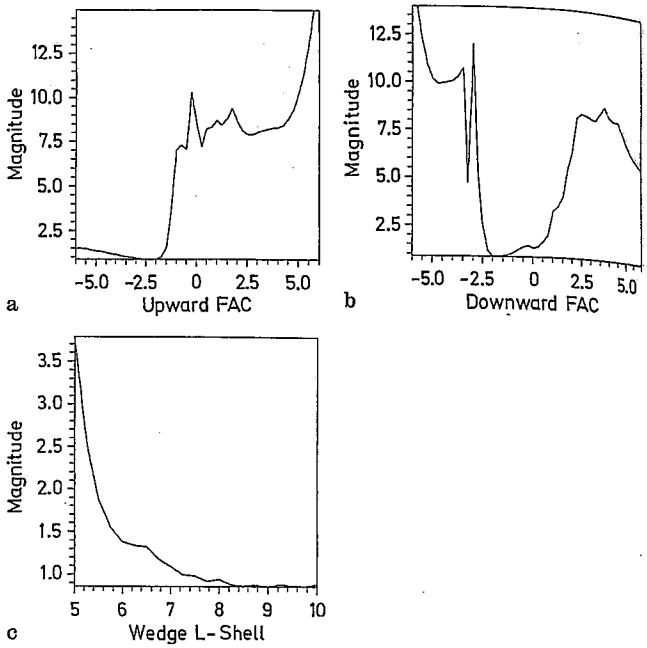

Fig. 15a–c. Model deviations projected onto each parameter axis for the first onset of the Day 258, 1988 event, with analysis of data from 01:44 to 01:49

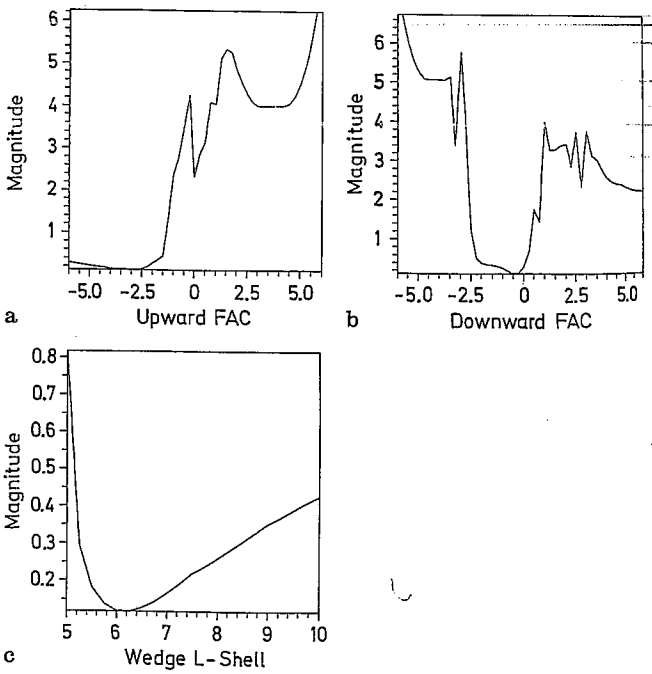

Fig. 16a–c. Model deviations projected onto each parameter axis for the second onset of the Day 258, 1988 event, with analysis of data from 01:51 to 01:57

(75%) gave results where the parameter set was well defined, and the current result was positive. Of the remaining events, 3 had well-defined FAC meridians but poorly defined *L*-shells and 4 gave ambiguous results, that is, the best fitting point bore little similarity to the best fitting

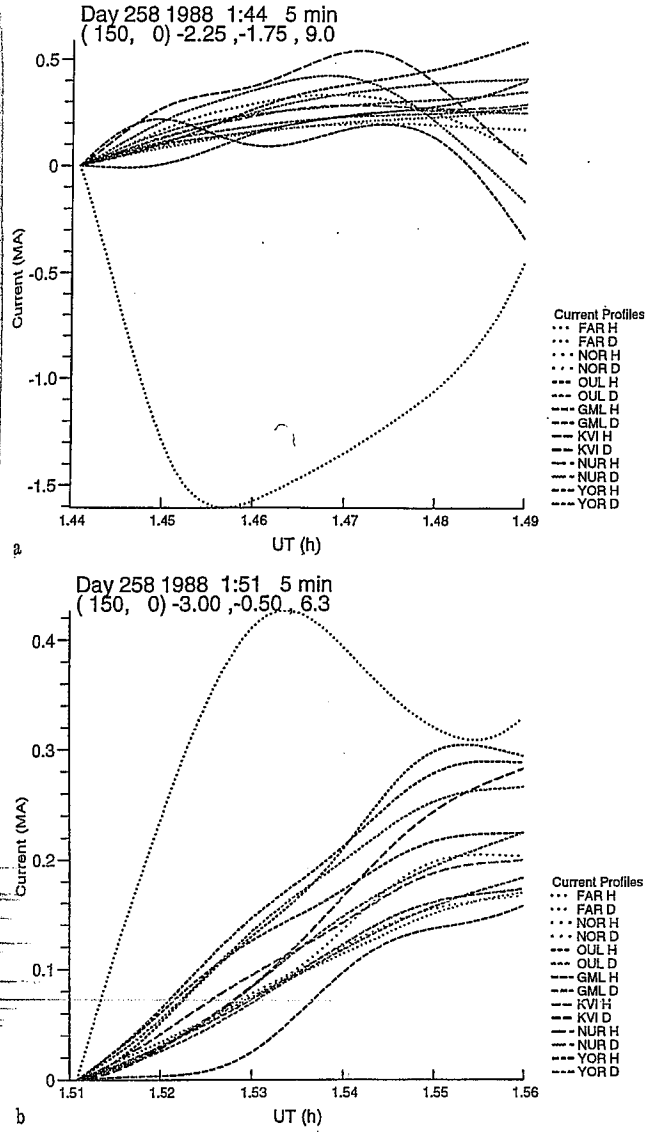

Fig. 17a, b. Superimposed current profiles for **a** the first, and **b** the second onsets of the Day 258, 1988 01:44 event

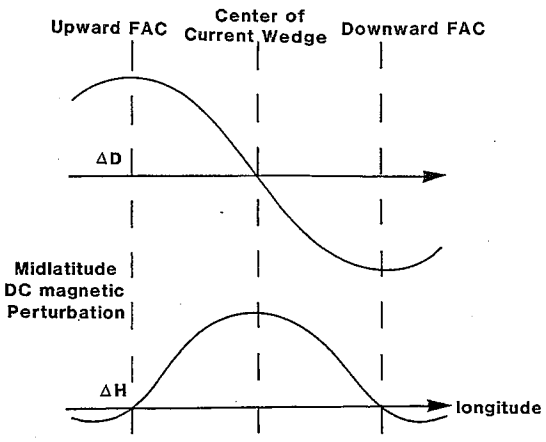

Fig. 18. Locations of zero ground field for a simple model current system. The positions of the FACs are indicated by zero *H*-component, and the centre of the system by zero D-component

trend. This would indicate that other current effects were overriding the substorm-associated current wedge in their influence on the model fitting. Six events gave negative currents, in other words, an eastward directed electrojet. However, of these 6 events, 3 identified the more distant of their two FACs at a meridian more than 5.5 h (82°) away from the array, which is at the limits of the ability of our model.

4.1 Field-aligned current meridians

In the past, certain specific features of the ground magnetograms have been taken as indicative of the meridians of the FACs. Lester *et al.* (1983, 1984, 1989) considered the positions where the *D*-component was zero as indicative of the central meridian of the wedge, and the positions of zero *H*-component at midlatitudes as indicating the meridians of the FACs (Fig. 18). The first assumption is true for any system having east-west symmetry, but the latter is only strictly true under the assumptions of widely separated, vertical FACs over a flat Earth, well away from the electrojet. A first step in comparing the method detailed in this paper with the other methods is to see whether it adequately predicts these features. If so then the associated parameter set is likely to be that much more reliable in that the above assumptions are not made.

The ground magnetic field deviations (ΔH and ΔD) for our 3D current wedge model are shown in Fig. 19. The zero deviation locations are marked with a heavy contour line. The vertical lines at -1.5 h, $+1.5$ h relative MLT correspond to the FAC longitudes, while the horizontal lines (i), (ii), and (iii) show the latitudes of our stations. While the stations at 61°N have their ΔH zero close to the correct MLT, the zero at 51°N is over one hour in MLT outside the wedge. This is also dependent on the *L*-shell position of the wedge relative to the station array.

For each wedge analysed, the expected ground field was computed on the basis of the best-fitting model parameter set, and for each meridional chain the expected positions of zero *H*- or *D*-component was derived. In Fig. 20 a comparison is made between these positions at the midlatitude stations (on the latitude of GML, KVI and NUR) and those measured from the experimental data. For the experimental data the positions of zero perturbation were inferred by fitting either a quadratic or a straight line to the data for each chain (dependent on the number of stations available) and hence calculating the zero intercepts. The SAMNET field-of-view occupies a region in the middle of the figure between -0.8 and $+1.0$ h local time and experimental values far from the SAMNET position are thus subject to extensive extrapolation. Ideally each event should yield two *H*-component zeros and one *D*-component zero. In practice the entire SAMNET array was not always available and sometimes the ground fields were ambiguous as to some or all of the positions, that is, after extrapolation there was sometimes no position of zero field deviation. A perfect agreement

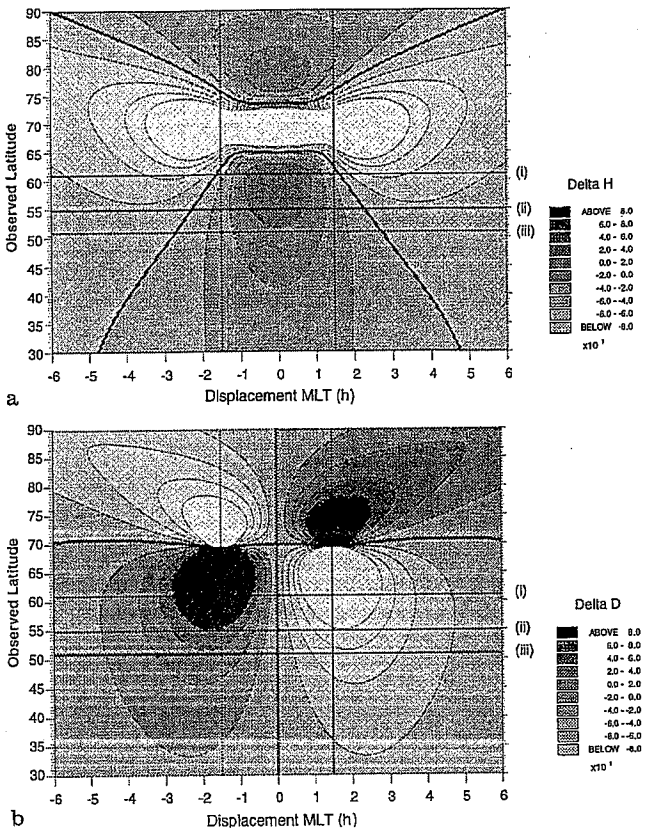

Fig. 19a, b. Ground field magnetic deviations due to a modelled 3D current wedge with upward FAC at −1.5 hours MLT, downward FAC at +1.5 h MLT (*vertical lines*), and *L*-shell of 8.0 (latitude ~68°N). *Horizontal lines* represent the latitudes of our stations: (i) FAR, NOR, OUL; (ii) GML, KVI, NUR; (iii) YOR. The locations of zero deviation are marked with a *heavy contour line*

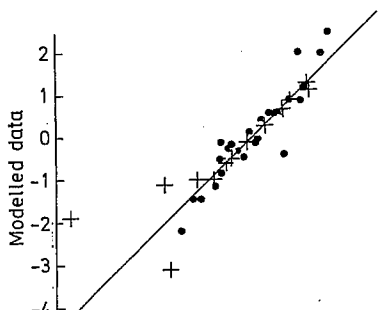

Fig. 20. Comparison between the meridians of zero *H*- and *D*-component variation extrapolated from midlatitude SAMNET data and inferred from the best-fitting parameter set. The circles represent *H*-component zeros and the crosses *D*-component zeros. The axis units are in hours of local time relative to the 90°E meridian. The least squares best fit has a gradient of 1.01

between modelled and experimental data would give a line of gradient 1. As can be seen, particularly in the vicinity of the SAMNET array there is a good agreement, with increasing scatter with increasing separation. The computed gradient of 1.01 has a correlation coefficient of 92% across a sample of 51 measurements.

If this plot is separated out into the contributions from the *H*- and *D*-components then the *H*-component gradient of 1.23 compares with the *D*-component gradient of 0.81. Thus the method tends to slightly overestimate the distance to *H*-zeros and underestimate that to *D*-zeros.

A similar procedure may be applied to the stations of the northern SAMNET chain (FAR, NOR and OUL), in which case Fig. 21 results. The scatter in this case is considerably greater than for the midlatitude data reflecting the more variable nature of these observations, but the average gradient is still 0.97 with a correlation coefficient of 85% over the sample of 44 measurements.

Thus the results appear to satisfactorily predict the longitudes where the *H*- and *D*-components are zero. The method of Lester *et al.* (1983, 1984, 1989) based on its 2D model would have assigned these as the meridians of the FACs and the centre of the wedge respectively, but the method employed here allows for the fact that the meridian of the *H*-component zero (Fig. 19) moves away from the central meridian of the wedge for latitudes away from the auroral zone (Lester *et al.*, 1989).

4.2 L-shell determination

Of the 52 events analysed, in 17 cases data were also available from the EISCAT Magnetometer Cross. In this section a comparison is made between the latitudes of zero *Z*-component as measured from this array, and those predicted from the model parameters as derived from the SAMNET array.

Between the meridians of the FACs the latitude of zero *Z*-component does not vary significantly from the latitude of the electrojet. Outside of these meridians, however, this latitude becomes a strong function of longitude, and as such is very sensitive to slight changes in the FAC positions. With this in mind, any events where the EISCAT magnetometer array was more than 1 h (15°) outside of the modelled wedge were discarded, leaving 11 usable events. Figure 22 gives the results of this analysis, through consideration of the distribution of errors. The first bar represents events where the zero of the *Z*-component did

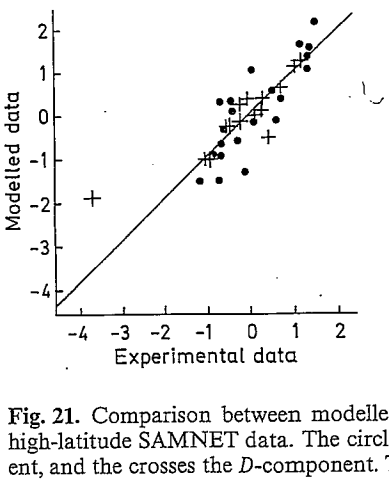

Fig. 21. Comparison between modelled zero field deviations and high-latitude SAMNET data. The circles represent the *H*-component, and the crosses the *D*-component. The least squares gradient is 0.97

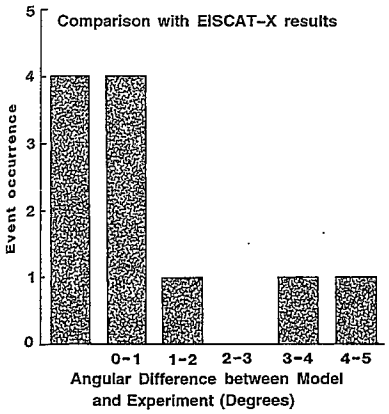

Fig. 22. Comparison between the latitude of zero Z-component as measured by the EISCAT Magnetometer Cross, and that inferred from the model parameter set best fitting the SAMNET data alone. The *bars* indicate the number of events where the angular difference was in the specified range. The first bar represents those events in which, from the EISCAT Cross data alone, it was only possible to determine whether the zero Z latitude was poleward or equatorward of the magnetometer array. In all these cases the model agreed with this position

not occur within the extremes of the available magnetometers so that all that could be concluded was whether the zero was at a higher or lower latitude than the array. For each of the 4 events in this category the locations of zero field were consistent with the modelled results though it is not possible to quantify the accuracy. The remaining bars indicate how accurate the fit was where the EISCAT array was able to detect the sign reversal. Four events gave modelled results within 1° of the experimental result, and 1 event gave results in each of the ranges 1°–2°, 3°–4° and 4°–5°.

5 Discussion

One of the major problems when investigating the gross field changes during substorms in the past has been the determination of a baseline from which to make measurements. The period prior to substorm onset is often disturbed, which can make any assumption of a 'zero' from which to make measurements a poor one. The procedure outlined in this paper does not make this assumption. A general offset at the start point simply shifts the intercept of the best-fit line relevant to a station pair and since it is the gradient of such a plot that is used this does not matter. Equally, a short-lived fluctuation which happened to coincide with the start of the measurement should have little effect on the average gradient calculated over a longer interval.

Given that a current wedge is being used to model the substorm current system, when trying to directly determine all parameters of a model current system in one step the data is not always adequate to the task. This method only entails the optimisation of three model parameters in the first stage, rather than the four of direct methods. It may be hoped that this should lead to a more reliable estimate. It also benefits from not needing to make any assumptions regarding the form of the inherently time-dependent fourth parameter, the current variation.

In comparison with the method of Lester *et al.* (1983, 1984, 1989), as demonstrated in Fig. 20, the method is quite able to generate a parameter set which successfully models the positions of zero field deviation. The assumptions detailed earlier are not made, ensuring that these estimates are more reliable. In addition, as a further indication of the method's success; it also satisfactorily models the positions of zero field deviation along the higher latitude SAMNET chain. Historically, it has not been possible to infer much wedge information from such stations due to the highly variable topology of the auroral fields. The method does not seem to be unduly affected by this.

It is to a large extent immune to the effects of geomagnetic noise at any of the stations. Whereas in a direct fit of all the parameters any local effects would be taken into account, Eq. (2) and (3) demonstrate that between any pair of stations there tends to be a cancellation of the effects of the local disturbance.

Whatever method is used, there will always be events where for one reason or another it is not possible to resolve all the model parameters. In most cases the method still successfully resolves one or both of the other geometrical parameters. In addition, in such cases it is often able to determine reasonable limits to the unknown parameter even if the exact position is not known. For example, Fig. 12 from the analysis of the Day 100, 1988 event clearly indicates that the upward FAC is well to the west of the array.

There are, however, problems. Sometimes the form of the projected axis plots was such that we could not be sure of any of the model parameters. Two different geometries would be likely to lead to such a situation, either a very wide wedge completely including the whole array, or a very narrow wedge well to one side of the array. Both cases would lead to only a slight variation across the observational array, the only distinguishing features being due to the electrojet section of the system. This element alone, however, has almost no effect on the D-component, and as such if it happened that several of the available stations were situated in regions where the H-component was small the method may be left with virtually nothing to distinguish between the above two cases. In such instances there is always a clear indication that there are no significant FACs close to the array, but there is an ambiguity over whether any currents are both to one side, on either side, or not present at all.

When a wedge analysis interval is chosen to coincide with a strong pulsation, the wedge position is nearly always found. However, if an onset is poorly defined then the procedure often identifies a wedge symmetrical about the array. This probably corresponds to a fit being made to the non-substorm associated electrojet alone which the method is mistaking for a part of a complete wedge system.

In both of the above cases, however, the value of the MWMSD was always large, indicating an unsatisfactory fit. As such it is not possible to be deceived into believing that such configurations are true and accurate

descriptions of the substorm current system. All that may be concluded is that such events are not amenable to analysis by this method.

Acknowledgements. The SAMNET data were supplied by Dr D. K. Milling (University of York, UK). We are grateful to Dr T. K. Yeoman (University of Leicester, UK) for the identification of certain of the events used, and to Mr A. Gebbie (University of York, UK) for his help with the production of the figures contained in this paper. The EISCAT Magnetometer Cross is a joint enterprise of the Finnish Meteorological Institute, the Sodankyla Geophysical Observatory, and the Technical University Braunschweig, and we thank Dr H. Lühr for supplying the data. Two of us (MC, RB) were in receipt of SERC studentships during most of the work detailed herein.

Topical Editor C.-G. Fälthammar thanks G. Rostoker and H.J. Opgenoorth for their help in evaluating this paper.

References

Horning, B. L., R. L. McPherron, and D. D. Jackson, Application of linear inverse theory to a line current model of substorm current systems, *J. Geophys. Res.*, **79,** 5202–5210, 1974.

Kisabeth, J. L., and G. Rostoker, Modelling of three-dimensional current systems associated with magnetospheric substorms, *Geophys. J. R. Astron. Soc.*, **49,** 655–683, 1977.

Lester, M., W. J. Hughes, and H. J. Singer, Polarization patterns of Pi2 magnetic pulsations and the substorm current wedge, *J. Geophys. Res.*, **88,** 7958–7966, 1983.

Lester, M., W. J. Hughes, and H. J. Singer, Longitudinal structure in Pi2 pulsations and the substorm current wedge, *J. Geophys. Res.*, **89,** 5489–5494, 1984.

Lester, M., H. J. Singer, D. P. Smits, and W. J. Hughes, Pi2 pulsations and the substorm current wedge, *J. Geophys. Res.*, **94,** 17133–17141, 1989.

Lühr, H., S. Thurey, and N. Klocker, The EISCAT Magnetometer Cross, *Geophys. Surv.*, **6,** 305–315, 1984.

McPherron, R. L., C. T. Russell, and M. P. Aubry, Satellite studies of magnetospheric substorms on August 15, 1968. 9. Phenomenological model of substorms, *J. Geophys. Res.*, **78,** 3131–3149, 1973.

Richmond, A. D., and Y. Kamide, Mapping electrodynamic features of the high-latitude ionosphere from localized observations: technique, *J. Geophys. Res.*, **93,** 5741–5759, 1988.

Richmond, A. D., Y. Kamide, B.-H. Ahn, S.-I. Akasofu, D. Alcaydé, M. Blanc, O. de la Beaujardiere, D. S. Evans, J. C. Foster, E. Friis-Christensen, T. J. Fuller-Rowell, J. M. Holt, D. Knipp, H. W. Kroehl, R. P. Lepping, R. J. Pellinen, C. Senior, and A. N. Zaitzev, Mapping electrodynamic features of the high-latitude ionosphere from localized observations: combined incoherent-scatter radar and magnetometer measurements for January 18–19, 1984, *J. Geophys. Res.*, **93,** 5760–5776, 1988.

Yeoman, T. K., *Substorm-associated pulsations: a study of plasmaspheric cavity resonance, mid-latitude polarisation and geostationary orbit signatures,* D. Phil. Thesis, University of York, 1988.

Yeoman, T. K., D. K. Milling, and D. Orr, Pi2 pulsation polarization patterns on the UK Sub-Auroral Magnetometer Network (SAMNET), *Planet. Space Sci.*, **38,** 589–602, 1990.